Photoelectron Spectroscopy and Computational Study on Microsolvated $[B_{10}H_{10}]^{2-}$ Clusters and Comparisons to their $[B_{12}H_{12}]^{2-}$ Analogues

Wenjin Cao[1, #], Zhubin Hu[2, #], Haitao Sun[2,3,4,*], Xue-Bin Wang[1,*]

[1] *Physical Sciences Division, Pacific Northwest National Laboratory, 902 Battelle Boulevard, P.O. Box 999, Richland, Washington 99352, United States*

[2] *State Key Laboratory of Precision Spectroscopy, School of Physics and Electronic Science, East China Normal University, Shanghai 200241, China*

[3] *Collaborative Innovation Center of Extreme Optics, Shanxi University, Taiyuan, Shanxi 030006, China*

[4] *NYU-ECNU Center for Computational Chemistry at NYU Shanghai, Shanghai, 200062, China*

[#] W. Cao and Z. Hu contributed equally to this work.

*Corresponding author. Email: xuebin.wang@pnnl.gov; htsun@phy.ecnu.edu.cn

ABSTRACT

Microhydrated *closo*-Boranes have attracted great interests due to their superchaotropic activity related to well-known Hofmeister effect and important applications in biomedical and battery fields. In this work, we report a combined negative ion photoelectron spectroscopy and quantum chemical investigation on hydrated *closo*-decaborate clusters $[B_{10}H_{10}]^{2-}\cdot nH_2O$ ($n = 1 – 7$) with a direct comparison to their analogues $[B_{12}H_{12}]^{2-}\cdot nH_2O$ and free water clusters. A single H_2O molecule is found sufficient to stabilize the intrinsically unstable $[B_{10}H_{10}]^{2-}$ dianion. The first two water molecules strongly interact with the solute forming B-H···H-O dihydrogen bonds while additional water molecules show substantially reduced binding energies. Unlike $[B_{12}H_{12}]^{2-}\cdot nH_2O$ possessing highly structured water network with the attached H_2O molecules arranged in a unified pattern by maximizing B-H···H-O dihydrogen bonding, distinct structural arrangements of the water clusters within $[B_{10}H_{10}]^{2-}\cdot nH_2O$ are achieved with the water cluster networks from trimer to heptamer resembling free water clusters. Such a distinct difference arises from the variations in size, symmetry, and charge distributions between these two dianions. The present finding again confirms the structural diversity of hydrogen-bonding networks in microhydrated *closo*-boranes and enrich our understanding of aqueous borate chemistry.

TOC Graphic

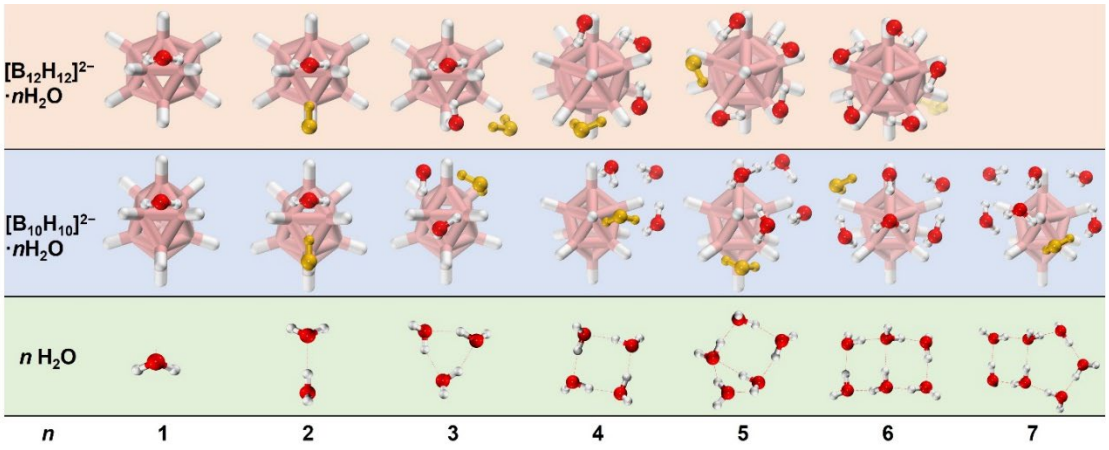

INTRODUCTION

closo-Boranes are well known for their broad applications in areas including boron-based neutron capture therapy and solid-state batteries[1-8] and have thus attracted numerous research interests. A variety of *closo*-polyhedral borate dianions $[B_nX_n]^{2-}$ with broad variations in vertex number n = 6–12 and ligand X = H, CN, or halogens, have been investigated, revealing substantial differences in their electronic structures, bonding properties, stability and reactivity.[9-15] Moreover, these dianions are classified as superchaotropic ions beyond the traditional Hofmeister scale,[16-17] exhibiting solute specificity[18-20] in electrolyte solutions and cross membrane transport. Therefore, their interactions with surrounding solvent molecules are an interesting topic to investigate, which is, however, much less studied. One effective approach to investigate such a topic is utilizing negative ion photoelectron spectroscopy (NIPES) on corresponding microsolvated clusters, which has been done for various Hofmeister ions.[20] To date, this has only been carried out for hydrated $[B_{12}H_{12}]^{2-}$ dianions and its halogenated derivatives,[21-22] and the complexes of $[B_{12}H_{12}]^{2-}$ binding to acetonitrile molecules[23] in the entire family of *closo*-borate dianions. No study on its closest analogue, *i.e.*, *closo*-decahydroborate $[B_{10}H_{10}]^{2-}$, whose physiochemical properties and interactions with surrounding solvents could be noticeably varied due to its smaller size, lower symmetry, nonuniform charge distribution and reduced polarizability,[24] has been carried out yet.

For the $[B_{12}H_{12}]^{2-}$ dianion, the water molecules attached have been identified to form a highly structured network due to preferrable B-H···H-O dihydrogen bonding.[21-22] The forming of dihydrogen bond (DHB) is attributed to a unique charge distribution where the H atoms outside of the boron core are negatively charged.[25] As a close analogue, $[B_{10}H_{10}]^{2-}$ is the second most stable *closo*-decahydroborates only after $[B_{12}H_{12}]^{2-}$ and among the most investigated hydroborates in the chemistry of the condensed phases.[26] It has a similar charge distribution with negative charged H atoms and a comparable size[27-28] in regard to $[B_{12}H_{12}]^{2-}$, a fact that would incline to a conclusion that $[B_{10}H_{10}]^{2-}$ may result in a similar solvation pattern and interactions with solvent molecules. On the other hand, substantial differences have been observed between these two dianions in the context of not only distinct electronic structures[28] but also different properties that guide their metabolic pathways.[29-30] Moreover, multiple previous studies have revealed nonuniform charge distribution on the ligand hydrogens of $[B_{10}H_{10}]^{2-}$,[27-28] which could affect its interaction with surrounding solvent molecules. The microsolvation pattern of the $[B_{10}H_{10}]^{2-}$ dianion and the comparison to that of $[B_{12}H_{12}]^{2-}$ are therefore of interest and remain to be explored.

In this work, we provide an answer to this question by a joint NIPES and quantum chemical computational study of $[B_{10}H_{10}]^{2-}\cdot nH_2O$ (n = 1 – 7) clusters. Although the $[B_{10}H_{10}]^{2-}$ dianion is known to be electronically unstable by itself in the gas phase,[28] one single H_2O molecule is found to sufficiently stabilize it albeit barely. The measured NIPE spectra provide key and sensitive experimental benchmarks, *e.g.*, vertical detachment energies (VDEs) and the corresponding stepwise shifts in VDEs (ΔVDEs) with each of the attached H_2O molecules for isomer identification.[22, 31] Referencing with high-level theoretical calculations, low-lying isomers of $[B_{10}H_{10}]^{2-}\cdot nH_2O$ complexes are then determined, revealing a different growth pattern in water networks organized by $[B_{10}H_{10}]^{2-}$compared to that of $[B_{12}H_{12}]^{2-}\cdot nH_2O$.[22] The configurations of H_2O clusters within $[B_{10}H_{10}]^{2-}\cdot nH_2O$ complexes are also compared with the corresponding well-studied free H_2O clusters.[32-36] Herein, we demonstrate that the nonuniform charge distribution in $[B_{10}H_{10}]^{2-}$ has significantly altered its solvation pattern with respect to $[B_{12}H_{12}]^{2-}$.

METHODS

Negative Ion Photoelectron Spectroscopy

The NIPES experiments were carried out using a magnetic-bottle time-of-flight (TOF) photoelectron spectrometer combined with an electrospray ionization (ESI) source and a temperature-controlled cryogenic ion trap, as described elsewhere.[37] The microsolvated $[B_{10}H_{10}]^{2-}$ cluster anions were generated by electrospraying ~1 mM solutions of its tetrabutylammonium salt dissolved in a acetonitrile/water (3:1 v/v) mixture solvent under humidity controlled environment. The resulting anions were transported by a radio frequency quadrupole ion guide, and first detected by a quadrupole mass spectrometer, during which the ESI conditions were optimized to ensure a stable and intense ion cluster beam. A 90˚ bender was used to direct the anions into the cryogenic 3D ion trap where they were accumulated for 20 – 100 ms and cooled by collisions with a cold buffer gas (20% H_2 balanced in He) to 20 K, before being pulsed-out into the extraction zone of the TOF mass spectrometer for mass analysis at a repetition rate of 10 Hz. Desired complex anions were each mass-selected and decelerated before being photodetached by a probe laser beam in the interaction zone of the magnetic-bottle photoelectron analyzer. A 157 nm (7.867 eV, Lambda Physik CompexPro F_2) laser beam, operated at a 20 Hz repetition rate with the anion beam shut off on alternating laser shots to afford shot-to-shot background subtraction, was used for

photodetachment. The resulting photoelectrons were collected at nearly 100% efficiency in the magnetic-bottle and analyzed with a 5.2-m-long electron flight tube. Recorded flight times were converted into kinetic energies calibrated using the known spectra of $I^-/OsCl_6^{2-}$.[38,39] The electron binding energy (EBE) spectra were obtained by subtracting the electron kinetic energies from the detachment photon energy with an electron energy resolution ($\Delta E/E$) of about 2% (*i.e.*, ~20 meV for 1 eV kinetic energy electrons).

Computational Details

The lowest-energy structures and corresponding low-lying isomers of $[B_{10}H_{10}]^{2-}\cdot nH_2O$ (n = 0 – 7) clusters were obtained by our home-built HydClus code. Firstly, an iterative sampling strategy to generate initial configurations of clusters was performed by genmer code[40] and followed by subsequent semi-empirical GFN2-xTB[41] optimizations using CREST code.[42] Single-point (SP) energy calculations were performed at the r^{2}SCAN-3c[43] level and hundreds to thousands of low-lying configurations were selected according to their SP energy levels. Secondly, the retained configurations of clusters were further optimized at the r^{2}SCAN-3c level, with their SP energies refined at the long-range corrected double-hybrid ωB97X-2-D3(BJ)[44]/ma-def2-TZVPP[45] level. Dozens to hundreds of low-energy configurations were thus selected accordingly. Thirdly, the retained configurations were further optimized at the PBE0[46]-D3(BJ)[47]/ma-def2-TZVP(-f)[45] level, followed by their SP energies refined at the ωB97X-2-D3(BJ)/ma-def2-QZVPP[45] level. Several to dozens of low-lying structures were selected into the final step accordingly. Finally, geometry optimizations for selected structures were reperformed using the PBE0-D3(BJ) functional with a larger aug-cc-pVTZ[48] basis set by Gaussian 16 software.[49] Vibrational frequencies were computed at the same level to ensure no imaginary frequencies. The VDEs were calculated at the DLPNO-CCSD(T)[50]/aug-cc-pVTZ level and obtained as the energy differences between the detached monoanions and corresponding dianions based on their dianions' optimized geometries. All the r^{2}SCAN-3c, ωB97X-2-D3(BJ) and DLPNO-CCSD(T) calculations were carried out by ORCA 5.0.4 software.[51] The restrained electrostatic potential (RESP)[52] charges of isolated $[B_{10}H_{10}]^{2-}$ were obtained using Multiwfn program.[53] To reveal the nature of intermolecular interactions between $[B_{10}H_{10}]^{2-}$ and water molecule, energy decomposition analysis (EDA) based on symmetry-adapted

perturbation theory (SAPT) at the SAPT2+[54,55]/aug-cc-pVDZ[48] level for $[B_{10}H_{10}]^{2-}\cdot H_2O$ cluster was conducted using PSI4 program.[56]

RESULTS AND DISCUSSION

NIPE spectra of $[B_{10}H_{10}]^{2-}\cdot nH_2O$ (n = 1 – 7) clusters

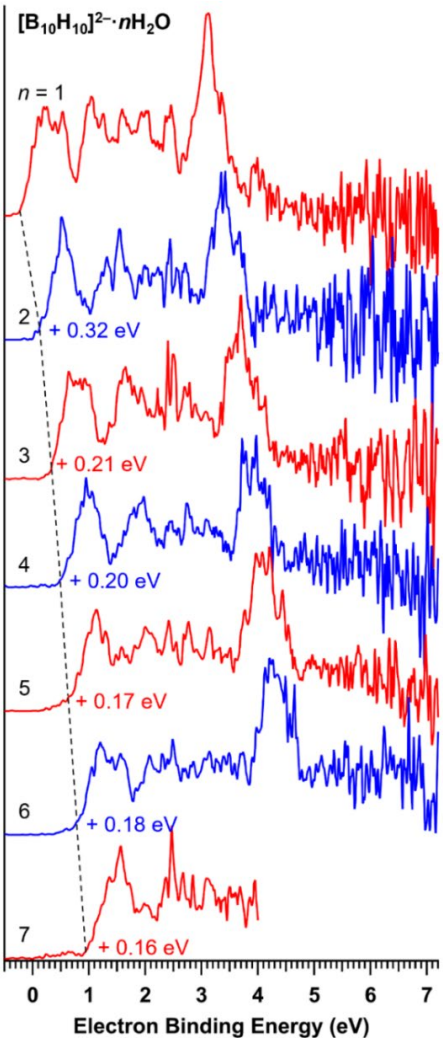

Figure 1 Cryogenic (20 K) NIPE spectra of $[B_{10}H_{10}]^{2-}\cdot nH_2O$ (n = 1 – 7) clusters recorded at 157 nm. The noisy spikes with EBEs above 4.5 eV that are due to imperfect background subtraction are scaled down by a factor of 0.3 to enhance the sake of clarity while the spectrum of $[B_{10}H_{10}]^{2-}\cdot 7H_2O$ is truncated above 4 eV due to the interference from the $[H\cdot B_{10}H_{10}]^-$ ion pair with a nearly-identical *m/z* ratio (see Figure S1 for a complete spectrum). The dashed lines and numbers indicate stepwise shifts in EBE.

Isolated $[B_{10}H_{10}]^{2-}$ dianion is an unstable fleeting species with a negative EBE and could not be detected in the gas phase.[28] Upon spraying under mild and humid conditions, a series of its hydrates $[B_{10}H_{10}]^{2-}\cdot nH_2O$ starting with $n = 1$ appeared, suggesting that a single water molecule is sufficient to stabilize the dianion leading the monohydrate detectable. The NIPE spectra of $[B_{10}H_{10}]^{2-}\cdot nH_2O$ ($n = 1 - 7$) clusters were measured with 157 nm incident photons (**Figure 1**), displaying 4-5 resolved broad bands spanning over 4 eV range with similar spectral patterns, while stepwise shifted to higher EBE with each additional H_2O molecule attached. The $[B_{10}H_{10}]^{2-}\cdot H_2O$ complex exhibits a VDE of 0.19 eV and a slightly negative (-0.05 eV) adiabatic detachment energy (ADE) estimated from the onset threshold of the first band, followed by a series of spectral bands up to an EBE of 4.5 eV (**Figure 1** and **Table 1**). All higher EBE features are suppressed due to the existence of a repulsive Coulomb barrier, which is a characteristic phenomenon in photodetaching multiply charged anions.[57,58] Due to the instability of isolated $[B_{10}H_{10}]^{2-}$ dianion, its experimental VDE is unavailable. Computed with the high-level DLPNO-CCSD(T) method, it possesses a VDE of -0.17 eV which is identical to the CCSD(T)-calculated one in a previous work.[28] Thus the 'experimental' ΔVDE upon addition of the first H_2O molecule is estimated to be 0.36 eV, which is comparable to that of 0.35 eV based on the same level of calculations (**Table 1**) and larger than the corresponding ΔVDE = 0.31 eV for the $[B_{12}H_{12}]^{2-}$ dianion.[22] With the second H_2O molecule added, VDE of $[B_{10}H_{10}]^{2-}\cdot 2H_2O$ is further shifted to 0.51 eV, with a ΔVDE of 0.32 eV which is also larger than the corresponding value for $[B_{12}H_{12}]^{2-}$ (0.27 eV). A substantially smaller ΔVDE of 0.21 eV is then observed for the $[B_{10}H_{10}]^{2-}\cdot 3H_2O$ cluster, when the observed ΔVDE reaches a "plateau" and remains similar for larger clusters, i.e., 0.20, 0.17, 0.18, and 0.16 eV for those with 4 to 7 water molecules attached, respectively (**Table 1** and **Figure 2**). It should be pointed out that the presented spectrum for $[B_{10}H_{10}]^{2-}\cdot 7H_2O$ is truncated at an EBE of 4 eV since it suffers strong interference from the $[H\cdot B_{10}H_{10}]^-$ ion pair with a similar *m/z* ratio. Nevertheless, the low EBE range is free from interference (**Figure S1**) and we are still able to determine a precise VDE for the $[B_{10}H_{10}]^{2-}\cdot 7H_2O$ complex.

Assuming the VDE of isolated $[B_{10}H_{10}]^{2-}$ dianion as the computed value of -0.17 eV, the total shift in VDE with first six H_2O molecules added is 1.44 eV for $[B_{10}H_{10}]^{2-}$ compared to that of 1.38 eV for $[B_{12}H_{12}]^{2-}$,[22] indicating similar strengths in ion-solvent interactions between these two dianions. The slightly stronger interaction strengths of $[B_{10}H_{10}]^{2-}$ with solvent water molecules, particularly for the first two water, qualitatively agrees with its smaller size and thus more negative

charge density (*vide infra*). **Figure S2** compares the ΔVDE trend between these two dianions. For $[B_{12}H_{12}]^{2-}$, the first five H_2O molecules are found forming a highly structured pattern whereas the sixth H_2O molecule separately attaches to the other side of the $[B_{12}H_{12}]^{2-}$ core, all driven by maximizing B-H···H-O DHB interactions. Accordingly, the observed ΔVDE exhibits a gradually descending trend for clusters with first five H_2O molecules attached and a noticeable increase for the $[B_{12}H_{12}]^{2-}\cdot 6H_2O$ complex (**Figure S2**).[22] In contrast, there is not a bounce in ΔVDE observed for the $[B_{10}H_{10}]^{2-}$ dianion, even with the seventh H_2O molecule attached (**Figure 2**). While $[B_{10}H_{10}]^{2-}$ exhibits stronger interactions with water than $[B_{12}H_{12}]^{2-}$ does for the first two H_2O molecules, the situation is reversed for the larger clusters (n = 3 – 6) where ΔVDEs of $[B_{12}H_{12}]^{2-}$ overtake those of $[B_{10}H_{10}]^{2-}$ except for n = 5, resulting in an overall weaker accumulative interaction for the latter in the range of n = 3 – 6. Unlike $[B_{12}H_{12}]^{2-}$ with a high I_h symmetry and a uniform charge distribution, the $[B_{10}H_{10}]^{2-}$ dianion adopts a D_{4d} symmetry and is known to possess two different types of B atoms (axial and equatorial) and distinctively two different charge distributions over the corresponding B-H bonds.[28] The different ΔVDE revolution pattern observed in $[B_{10}H_{10}]^{2-}$ does indicate a different solvation mechanism compared to that of $[B_{12}H_{12}]^{2-}$. To shed light on these differences, quantum chemical calculations have been carried out to reveal the solvation mechanism of $[B_{10}H_{10}]^{2-}$.

Table 1. Comparisons of experimental (expt., eV) and DLPNO-CCSD(T)-calculated (calc., eV) VDEs and stepwise shifts in VDEs (ΔVDEs) of $[B_{10}H_{10}]^{2-}\cdot nH_2O$ (n = 1 – 7) clusters.

n =	expt. VDE	expt. ΔVDE	calc. VDE	calc. ΔVDE
0	–		-0.17	
1	0.19	0.36[a]	0.18	0.35
2	0.51	0.32	0.49	0.31
3	0.72	0.21	0.67	0.19
4	0.92	0.20	0.87	0.20
5	1.09	0.17	1.08	0.21
6	1.27	0.18	1.28	0.20
7	1.43	0.16	1.47	0.19

[a] Obtained by subtracting the calculated VDE of $[B_{10}H_{10}]^{2-}$ (-0.17 eV) from the experimental VDE of $[B_{10}H_{10}]^{2-}\cdot H_2O$ (0.19 eV).

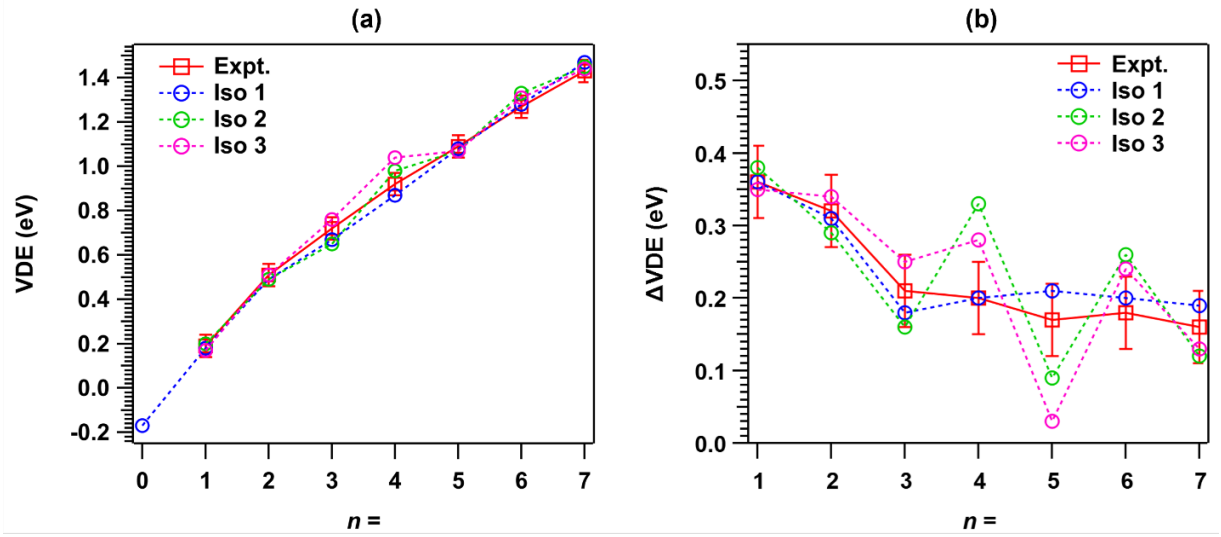

Figure 2. Experimental (expt., red) and DLPNO-CCSD(T)-calculated (blue - iso 1, green - iso 2, and pink - iso 3) VDEs (a) and ΔVDEs (b) of $[B_{10}H_{10}]^{2-}\cdot nH_2O$ (n = 1 – 7).

Optimized low-lying structures and calculated VDEs / ΔVDEs

The optimized isolated $[B_{10}H_{10}]^{2-}$ dianion adopts a D_{4d} symmetry with two tetrahedral pyramidal units stacking together at a rotated angle of 45° (**Figure 3**). Two B atoms sit along the long axis (axial B_{ax}), each bonded to four equatorial ones (B_{eq}) at 1.699 Å, while eight B atoms form an equatorial bell, each fivefold bonded to its neighboring B atoms. The bond length between adjacent equatorial B atoms within the same pyramid, i.e., B7-B8, is 1.830 Å, while that of the two B atoms from different pyramids, i.e., B4-B9, is slightly shorter at 1.811 Å. Though minor differences observed in B-H bond lengths between those at axial and equatorial positions (1.203 Å for axial and 1.208 Å for equatorial), these two types of H atoms carry substantially different amounts of negative charges (**Figure 3**). Each of the two axial B atoms with a 4-inner cluster connectivity possesses slightly negative charge of -0.178 based on the RESP charge analysis and the corresponding axial H atom also negatively charged at -0.193. In contrast, each equatorial B atom with 5 inner cluster connectivity is positively charged (+0.089), rendering the H atom it connected to with more negative charge (-0.246), which is ~30% more negative than those at the axial position. Each equatorial H atom in $[B_{10}H_{10}]^{2-}$ also holds more negative charges than that in $[B_{12}H_{12}]^{2-}$ (computed as -0.228 per each at the same level of theory, **Figure S3**). These partial negative charges on the H atoms make them ideal hydrogen bond acceptors to form DHBs with

H_2O molecules, as shown in the previous studies on microsolvated $[B_{12}H_{12}]^{2-}$.[21,22] Based on the DLPNO-CCSD(T) calculations, the $[B_{10}H_{10}]^{2-}$ dianion is unstable with a negative VDE of -0.17 eV (**Table 1**), consistent with the fact that it could not be experimentally observed.

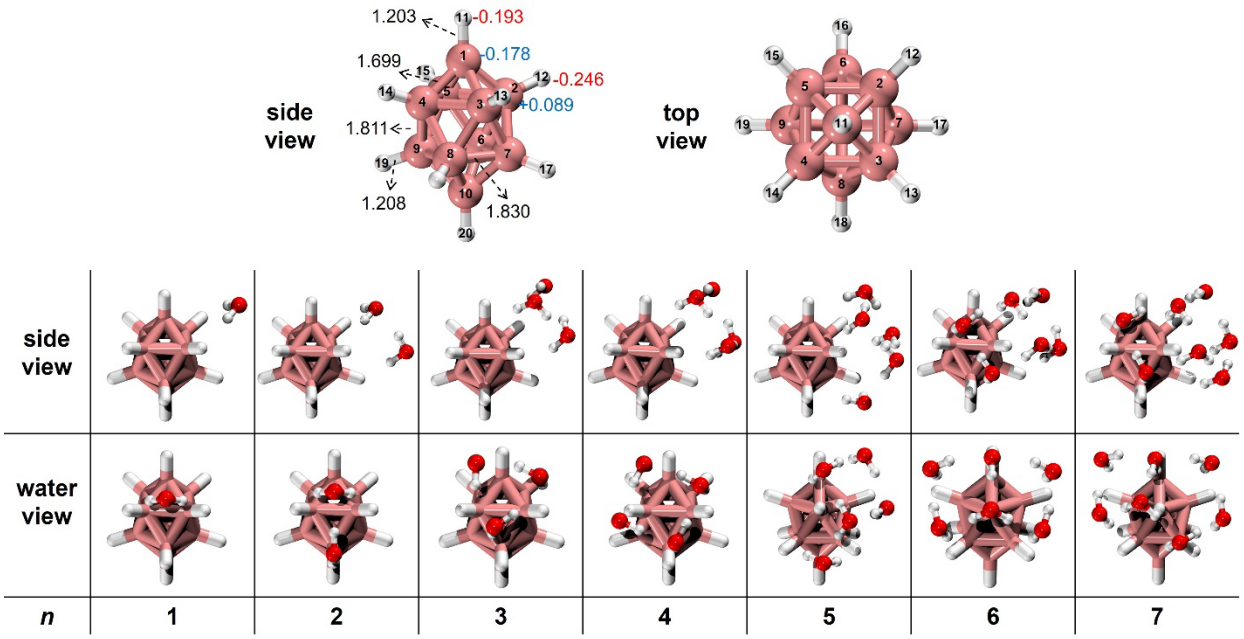

Figure 3. Optimized lowest-lying structures of $[B_{10}H_{10}]^{2-}\cdot nH_2O$ (n = 0 – 7) clusters. The numbers on isolated $[B_{10}H_{10}]^{2-}$ indicate the atomic labels in this work. The bond lengths (Å, black) and RESP charges (*e*, blue for B and red for H) of isolated $[B_{10}H_{10}]^{2-}$ are also listed.

Since more negative charges populate at the equatorially positioned H ligands, the first H_2O molecule is expected to attach to equatorial B-Hs via forming a bidentate DHB. The most stable monohydrate features a H_2O molecule bound to two adjacent equatorial B-H bonds within the same pyramid and possesses a calculated VDE of 0.18 eV, in excellent agreement with the experimentally measured value of 0.19 eV. Taking the computed VDE of -0.17 eV for the isolated $[B_{10}H_{10}]^{2-}$, the calculated VDE shift induced by the first water is ΔVDE = 0.35 eV, compared well to the experimental value of 0.36 eV (**Table 1**), both noticeably larger than the corresponding experimental ΔVDE = 0.31 eV for $[B_{12}H_{12}]^{2-}$.[22] Accordingly, the 1st water binding energy computed at the SAPT2+/aug-cc-pVDZ level amounts to 15.79 kcal/mol, also being higher than that of 14.31 kcal/mol for $[B_{12}H_{12}]^{2-}\cdot H_2O$, which is mainly attributed to the enhanced electrostatic

interaction based on energy decomposition analysis (**Figure S4**). Such a difference parallels with the predicted slightly more negative charge on the equatorial H atoms in $[B_{10}H_{10}]^{2-}$. The second lowest-lying isomer (isomer 2) of $[B_{10}H_{10}]^{2-}\cdot H_2O$ with the H_2O molecule bridging one B_{eq}-H and its adjacent B_{ax}-H bond (**Figure S5**) is 0.35 kcal/mol higher in energy and has a higher computed VDE of 0.20 eV (**Table S1**). A third isomer (isomer 3) with the H_2O bound to two B_{eq}-H groups but in different pyramid is also located with an even higher relative energy of 0.61 kcal/mol and a smaller calculated VDE of 0.17 eV.

With the first H_2O molecule attached to B2-H and B3-H (two equatorial B-H in the same pyramid), the second H_2O molecule is found to bind to the first H_2O and another B-H group. Two nearly isoenergic isomers are identified for the $[B_{10}H_{10}]^{2-}\cdot 2H_2O$ complex (**Figure 3** and **S5**), where isomer 1 with the 2nd H_2O attached to another equatorial B7-H is only 0.01 kcal/mol more stable compared to isomer 2, in which the 2nd water is attached to the axial B1-H. They also possess an identical calculated VDE 0.49 eV. Isomer 3 of the dihydrate evolves from isomer 2 of the monohydrate with the 1st H_2O molecule attached to B3-H (equatorial) and B1-H (axial), the 2nd H_2O located at B2-H (equatorial in the same pyramid) and binding to the 1st H_2O molecule and is 0.78 kcal/mol higher in energy. With more H_2O molecules added, the competition between dihydrogen bonding (H_2O vs. $[B_{10}H_{10}]^{2-}$) and conventional hydrogen bonding (H_2O vs. H_2O) appears. The newly attached H_2O molecule tends to use one H atom to form DHB with the $[B_{10}H_{10}]^{2-}$ dianion whereas also interacting with other H_2O molecules, forming hydrogen bonded H_2O network (**Figure 3**). The calculated VDEs based on the three lowest-lying isomers all follow the experimental VDE trend well (**Figure 2a**) and seems to suggest that VDE is a less sensitive experimental benchmark for distinguishing different isomers. However, the differential of VDE, *i.e.*, $\Delta VDE(n) = VDE(n) - VDE(n\text{-}1)$ amplifies the subtle VDE differences between different isomers and, to a large degree, can cancel systematic errors in both measurements and calculations. As shown in **Figure 2b**, the calculated ΔVDEs based on the lowest-lying isomer 1 of each of the hydrated complexes exhibit substantially better agreements with the experimental ΔVDEs than those based on the next two isomers, indicating the dominant presence of the most stable isomers in our experiments. Moreover, it demonstrates that ΔVDE is a much more sensitive parameter being capable to distinguish various isomers.

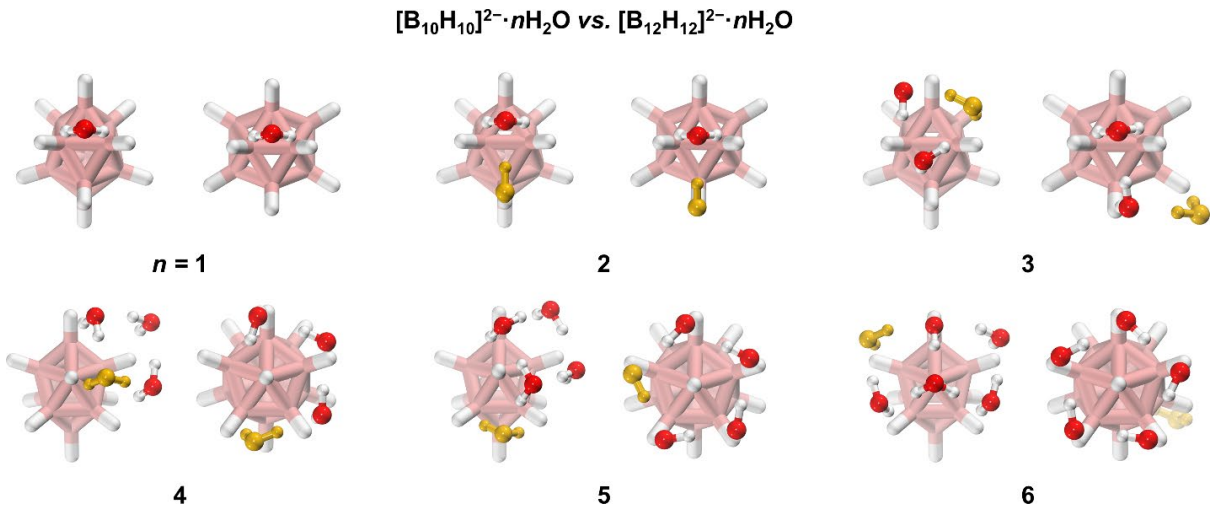

Figure 4. Schematic diagram for direct comparisons of the lowest-lying $[B_{10}H_{10}]^{2-}\cdot nH_2O$ and $[B_{12}H_{12}]^{2-}\cdot nH_2O$ (n = 1 – 6) conformations. The H_2O molecule in gold color represents the one newly attached.

Comparing $[B_{10}H_{10}]^{2-}$ vs $[B_{12}H_{12}]^{2-}$ microsolvation

It is fascinating to examine and compare the initial hydration process of $[B_{10}H_{10}]^{2-}$ against that of $[B_{12}H_{12}]^{2-}$ as both dianions are highly analogous while possess distinct differences in cluster size, symmetry, and charge distribution. Our previous study on microsolvated $[B_{12}H_{12}]^{2-}$revealed that the attached waters evolve into a unique, highly structured water network driven by maximizing the solute-solvent B-H···H-O DHB interaction, with the water pentamer being arranged in a nearly planar cyclic pattern while the 6th H_2O attaching from the other side of the $[B_{12}H_{12}]^{2-}$ core.[22] As shown in **Figure 4**, the binding motifs for the first two H_2O molecules with these two dianions are identical. Specifically, the 1st water forms a bidentate B-H···H-O DHB with the solutes albeit in the equatorial position for decaborate, and the 2nd H_2O forms one O···H-O HB with the first H_2O and one B-H···H-O DHB with the borate. The contrast solvation pattern between these two borates appears starting at $n \geq 3$. Different from $[B_{12}H_{12}]^{2-}\cdot 3H_2O$, in which the 3rd H_2O simultaneously interacts with the two previously attached water, significant water molecule rearrangement in $[B_{10}H_{10}]^{2-}\cdot 3H_2O$ appears by forming a three-membered water ring, a morphology similar to the free water trimer (**Figure S6**). A similar trend is observed for the $[B_{10}H_{10}]^{2-}\cdot 4H_2O$ complex in which a four-membered water ring is formed instead of an open-loop network as seen in $[B_{12}H_{12}]^{2-}\cdot 4H_2O$. While the 5th attached H_2O molecule constructs a closed-loop H_2O ring in

$[B_{12}H_{12}]^{2-}\cdot 5H_2O$, the $[B_{10}H_{10}]^{2-}\cdot 5H_2O$ complex has this molecule attached from outside of the four-membered ring formed in the previous complex. The next H_2O molecule also attaches outside of the ring just next to the 5th one, forming a "book" water conformation. Such a pattern is also different from that of $[B_{12}H_{12}]^{2-}\cdot 6H_2O$ with the newly added H_2O molecule attaching from the opposite side of the $[B_{12}H_{12}]^{2-}$ core, which is still not seen for $[B_{10}H_{10}]^{2-}\cdot 7H_2O$. These distinct differences in the context of the water network seen from trihydrate to hexahydrate vividly illustrate the solvation tunability brough upon by the subtle molecular property variations (*e.g.*, size and charge distribution) between these two borate dianions.

Interestingly, the patterns of water networks in $[B_{10}H_{10}]^{2-}\cdot n H_2O$ resemble those of isolated water clusters, *i.e.*, all adopting nearly identical cyclic patterns for n = 3 and 4 (**Figure 3** and **S6**).[32] Isolated water pentamer is known to form a five-membered ring with each H_2O molecule hydrogen bonded to each other,[32] whereas the H_2O molecules in $[B_{10}H_{10}]^{2-}\cdot 5H_2O$ form a four-membered ring with an extra one staying aside (**Figure 3**). A similar structure for the isolated $(H_2O)_5$ cluster was found to be only slightly higher in energy compared to the five-membered cyclic one and was detected in an infrared spectroscopic measurement[33] (**Figure S6**). Likewise, for the lowest energy isomer of $[B_{10}H_{10}]^{2-}\cdot n H_2O$ (n = 6, 7), each contains a water network that is known in isolated water hexamer and heptamer. Specifically, the water cluster in $[B_{10}H_{10}]^{2-}\cdot 6H_2O$ adopts a "book" conformation, calculated to be 0.74/0.49 kcal/mol higher in energy than the prism/cage configuration in the free $(H_2O)_6$ cluster, in line with multiple previous studies[32-36] showing similar energetic predictions. The "chair" conformation in $[B_{10}H_{10}]^{2-}\cdot 7H_2O$ also corresponds to a higher energy isomer for the isolated $(H_2O)_7$ cluster (**Figure S6**).[36] These higher energy water conformations benefit from the fairly strong intermolecular interactions with the $[B_{10}H_{10}]^{2-}$ dianion, becoming dominant in the $[B_{10}H_{10}]^{2-}\cdot n H_2O$ clusters.

CONCLUSIONS

In conclusion, microsolvated $[B_{10}H_{10}]^{2-}$ clusters were investigated via a combined NIPES and theoretical study, particularly with respect to its analogues $[B_{12}H_{12}]^{2-}$. Although the isolated $[B_{10}H_{10}]^{2-}$ dianion is unstable by itself in the gas phase, a single H_2O molecule is sufficient to make it stable enough to be detected. The recorded NIPE spectra of $[B_{10}H_{10}]^{2-}\cdot n H_2O$ (n = 1-7) provide precise VDEs and ΔVDEs of the hydrate clusters with each of H_2O molecules added. The trend in

ΔVDE, when compared to that of $[B_{12}H_{12}]^{2-}\cdot nH_2O$, indicates a distinctly different solvation mechanism. By referencing with high-level quantum chemical calculations, the lowest-lying isomer for each hydrate is identified, revealing the water networks in $[B_{10}H_{10}]^{2-}\cdot nH_2O$ (n = 3 – 7) contain morphologies similar to those found in the corresponding isolated $(H_2O)_n$ clusters albeit not being always the lowest-lying ones. This contrasts to the situation previously determined for $[B_{12}H_{12}]^{2-}\cdot nH_2O$, where the water molecules were arranged into highly structured cyclic networks by the $[B_{12}H_{12}]^{2-}$ core. This distinct difference observed in solvation mechanism between these two fairly similar *closo*-borate dianions is unexpected, exhibiting how sensitive the role of size and charge distribution is in organizing surrounding water networks. Lastly, the present findings once again demonstrate the structural diversity of hydrogen bonding-driven water networks in microhydrated boranes, and strengthen the molecular-level understanding of solute–solvent interactions for aqueous borate chemistry.

ASSOCIATED CONTENTS

Supporting Information

The Supporting Information is available free of charge at https://pubs.acs.org/doi/10.1021/acs.jpca.xxxxxxx.

A full NIPE spectrum of $[B_{10}H_{10}]^{2-}\cdot 7H_2O$ and its comparison to that of $[HB_{10}H_{10}]^{-}$, comparison in ΔVDEs between $[B_{10}H_{10}]^{2-}\cdot nH_2O$ and $[B_{12}H_{12}]^{2-}\cdot nH_2O$ clusters, calculated RESP charge distributions on B and H atoms for $[B_{10}H_{10}]^{2-}$ and $[B_{12}H_{12}]^{2-}$ dianions, energy decompositions of binding energies for $[B_{10}H_{10}]^{2-}\cdot H_2O$ and $[B_{12}H_{12}]^{2-}\cdot H_2O$ complexes at the SAPT2+/aug-cc-pVDZ level, three lowest lying isomers for $[B_{10}H_{10}]^{2-}\cdot nH_2O$ (n = 1 – 7) complexes, optimized geometries of low-lying conformations of $(H_2O)_n$ (n = 2 – 7) clusters at the MP2/aug-cc-pVDZ level.

AUTHOR INFORMATION

Corresponding Authors

Haitao Sun − *State Key Laboratory of Precision Spectroscopy, School of Physics and Electronic Science, East China Normal University, Shanghai 200241, China;*

Collaborative Innovation Center of Extreme Optics, Shanxi University, Taiyuan, Shanxi 030006, China; NYU-ECNU Center for Computational Chemistry at NYU Shanghai, Shanghai, 200062, China; orcid.org/0000-0003-1471-8876; Email: htsun@phy.ecnu.edu.cn

Xue-Bin Wang − *Physical Sciences Division, Pacific Northwest National Laboratory, 902 Battelle Boulevard, P.O. Box 999, Richland, Washington 99352, United States;* orcid.org/0000-0001-8326-1780; Email: xuebin.wang@pnnl.gov

Authors

Wenjin Cao − *Physical Sciences Division, Pacific Northwest National Laboratory, 902 Battelle Boulevard, P.O. Box 999, Richland, Washington 99352, United States*

Zhubin Hu − *State Key Laboratory of Precision Spectroscopy, School of Physics and Electronic Science, East China Normal University, Shanghai 200241, China*

Notes

The authors declare no competing financial interest.

ACKNOWLEDGMENTS

The NIPES work was supported by the U.S. Department of Energy (DOE), Office of Science, Office of Basic Energy Sciences, Division of Chemical Sciences, Geosciences, and Biosciences, Condensed Phase and Interfacial Molecular Science program, FWP 16248. The theoretical work was supported by the National Natural Science Foundation of China (Nos. 12274128, 12034008, 12250003, and 12204172), Shanghai Rising-Star Program (No. 21QA1402600), and the Program of Introducing Talents of Discipline to Universities 111 Project (B12024). We acknowledge the ECNU Multifunctional Platform for Innovation (001) and HPC Research Computing Team for providing computational and storage resources and the support of NYU-ECNU Center for Computational Chemistry at NYU Shanghai.

REFERENCES

(1) Hawthorne, M. F. The Role of Chemistry in the Development of Boron Neutron Capture Therapy of Cancer. *Angew. Chem. Int. Ed.* **1993,** *32*, 950-984.
(2) Hosmane, N. S., *Boron Science: New Technologies and Applications*. CRC Press: 2011.
(3) Giri, S.; Behera, S.; Jena, P. Superhalogens as Building Blocks of Halogen-Free Electrolytes in Lithium-Ion Batteries. *Angew. Chem. Int. Ed.* **2014,** *53*, 13916-13919.
(4) Tutusaus, O.; Mohtadi, R.; Arthur, T. S.; Mizuno, F.; Nelson, E. G.; Sevryugina, Y. V. An Efficient Halogen-Free Electrolyte for Use in Rechargeable Magnesium Batteries. *Angew. Chem. Int. Ed.* **2015,** *54*, 7900-7904.
(5) Tang, W. S.; Unemoto, A.; Zhou, W.; Stavila, V.; Matsuo, M.; Wu, H.; Orimo, S.-i.; Udovic, T. J. Unparalleled Lithium and Sodium Superionic Conduction in Solid Electrolytes with Large Monovalent Cage-Like Anions. *Energy Environ. Sci.* **2015,** *8*, 3637-3645.
(6) Zhao, H.; Zhou, J.; Jena, P. Stability of $B_{12}(CN)_{12}^{2-}$: Implications for Lithium and Magnesium Ion Batteries. *Angew. Chem. Int. Ed.* **2016,** *55*, 3704-3708.
(7) Payandeh, S.; Asakura, R.; Avramidou, P.; Rentsch, D.; Łodziana, Z.; Černý, R.; Remhof, A.; Battaglia, C. Nido-Borate/Closo-Borate Mixed-Anion Electrolytes for All-Solid-State Batteries. *Chem. Mater.* **2020,** *32*, 1101-1110.
(8) Ready, A. D.; Irshad, A.; Kallistova, A.; Carrillo, M.; Gembicky, M.; Seshadri, R.; Narayan, S.; Spokoyny, A. M. Electrochemical Cycling of Redox-Active Boron Cluster-Based Materials in the Solid State. *J. Am. Chem. Soc.* **2023,** *145*, 14345-14353.
(9) Aihara, J. Three-Dimensional Aromaticity of Polyhedral Boranes. *J. Am. Chem. Soc.* **1978,** *100*, 3339-3342.
(10) Otsuka, M.; Takita, R.; Kanazawa, J.; Miyamoto, K.; Muranaka, A.; Uchiyama, M. Conjugation between σ- and π-Aromaticity in 1-C-Arylated Monocarba-closo-dodecaborate Anions. *J. Am. Chem. Soc.* **2015,** *137*, 15082-15085.
(11) Axtell, J. C.; Saleh, L. M. A.; Qian, E. A.; Wixtrom, A. I.; Spokoyny, A. M. Synthesis and Applications of Perfunctionalized Boron Clusters. *Inorg. Chem.* **2018,** *57*, 2333-2350.
(12) Poater, J.; Escayola, S.; Poater, A.; Teixidor, F.; Ottosson, H.; Viñas, C.; Solà, M. Single—Not Double—3D-Aromaticity in an Oxidized Closo Icosahedral Dodecaiodo-Dodecaborate Cluster. *J. Am. Chem. Soc.* **2023,** *145*, 22527-22538.
(13) Warneke, J. Gas-Phase Ion Chemistry of $[B_{12}X_{12}]^{2-}$ (X = F, Cl, Br, I, CN). A Brief Review of Twelve Years of Researching Twelve−Vertexed Dianions and Their Fragments. *Int. J. Mass spectrom.* **2024,** *496*, 117169.
(14) Warneke, J.; Konieczka, S. Z.; Hou, G.-L.; Aprà, E.; Kerpen, C.; Keppner, F.; Schäfer, T. C.; Deckert, M.; Yang, Z.; Bylaska, E. J., et al. Properties of Perhalogenated {closo-B_{10}} and {closo-B_{11}} Multiply Charged Anions and a Critical Comparison with {closo-B_{12}} in the Gas and the Condensed Phase. *Phys. Chem. Chem. Phys.* **2019,** *21*, 5903-5915.
(15) Warneke, J.; Wang, X.-B. Measuring Electronic Structure of Multiply Charged Anions to Understand Their Chemistry: A Case Study on Gaseous Polyhedral closo-Borate Dianions. *J. Phys. Chem. A* **2021,** *125*, 6653-6661.
(16) Assaf, K. I.; Ural, M. S.; Pan, F.; Georgiev, T.; Simova, S.; Rissanen, K.; Gabel, D.; Nau, W. M. Water Structure Recovery in Chaotropic Anion Recognition: High-Affinity Binding of Dodecaborate Clusters to γ-Cyclodextrin. *Angew. Chem. Int. Ed.* **2015,** *54*, 6852-6856.
(17) Assaf, K. I.; Nau, W. M. The Chaotropic Effect as an Assembly Motif in Chemistry. *Angew. Chem. Int. Ed.* **2018,** *57*, 13968-13981.

(18) Tobias, D. J.; Hemminger, J. C. Getting Specific About Specific Ion Effects. *Science* **2008,** *319*, 1197-1198.
(19) Jungwirth, P.; Tobias, D. J. Specific Ion Effects at the Air/Water Interface. *Chem. Rev.* **2006,** *106*, 1259-1281.
(20) Wang, X.-B. Cluster Model Studies of Anion and Molecular Specificities via Electrospray Ionization Photoelectron Spectroscopy. *J. Phys. Chem. A* **2017,** *121*, 1389-1401.
(21) Jiang, Y.; Yuan, Q.; Cao, W.; Hu, Z.; Yang, Y.; Zhong, C.; Yang, T.; Sun, H.; Wang, X.-B.; Sun, Z. Unraveling Hydridic-to-Protonic Dihydrogen Bond Predominance in Monohydrated Dodecaborate Clusters. *Chem. Sci.* **2022,** *13*, 9855-9860.
(22) Jiang, Y.; Cai, Z.; Yuan, Q.; Cao, W.; Hu, Z.; Sun, H.; Wang, X.-B.; Sun, Z. Highly Structured Water Networks in Microhydrated Dodecaborate Clusters. *J. Phys. Chem. Lett.* **2022,** *13*, 11787-11794.
(23) Peng, X.; Cao, W.; Hu, Z.; Yang, Y.; Sun, Z.; Wang, X.-B.; Sun, H. Observation of a Super-Tetrahedral Cluster of Acetonitrile-Solvated Dodecaborate Dianion Via Dihydrogen Bonding. *J. Chem. Phys.* **2024,** *160*, 054308.
(24) Salluce, G.; Folgar-Cameán, Y.; Barba-Bon, A.; Nikšić-Franjić, I.; El Anwar, S.; Grüner, B.; Lostalé-Seijo, I.; Nau, W. M.; Montenegro, J. Size and Polarizability of Boron Cluster Carriers Modulate Chaotropic Membrane Transport. *Angew. Chem. Int. Ed.* **2024**, e202404286.
(25) Aprà, E.; Warneke, J.; Xantheas, S. S.; Wang, X.-B. A Benchmark Photoelectron Spectroscopic and Theoretical Study of the Electronic Stability of $[B_{12}H_{12}]^{2-}$. *J. Chem. Phys.* **2019,** *150*, 164306.
(26) Sivaev, I. B.; Prikaznov, A. V.; Naoufal, D. Fifty Years of the closo-Decaborate Anion Chemistry. *Collect. Czech. Chem. Commun.* **2010,** *75*, 1149-1199.
(27) Mahfouz, N.; Ghaida, F. A.; El Hajj, Z.; Diab, M.; Floquet, S.; Mehdi, A.; Naoufal, D. Recent Achievements on Functionalization within closo-Decahydrodecaborate $[B_{10}H_{10}]^{2-}$ Clusters. *ChemistrySelect* **2022,** *7*, e202200770.
(28) Cao, W.; Warneke, J.; Wang, X.-B. Probing the Electronic Structure of $[B_{10}H_{10}]^{2-}$ Dianion Encapsulated by an Octamethylcalix[4]pyrrole Molecule. *J. Phys. Chem. A* **2024,** *128*, 3361-3369.
(29) Soloway, A. H.; Tjarks, W.; Barnum, B. A.; Rong, F.-G.; Barth, R. F.; Codogni, I. M.; Wilson, J. G. The Chemistry of Neutron Capture Therapy. *Chem. Rev.* **1998,** *98*, 1515-1562.
(30) Wilbur, D. S.; Chyan, M.-K.; Hamlin, D. K.; Perry, M. A. Reagents for Astatination of Biomolecules. 3. Comparison of closo-Decaborate(2-) and closo-Dodecaborate(2-) Moieties as Reactive Groups for Labeling with Astatine-211. *Bioconjugate Chem.* **2009,** *20*, 591-602.
(31) Cao, W.; Wen, H.; Xantheas, S. S.; Wang, X.-B. The Primary Gas Phase Hydration Shell of Hydroxide. *Sci. Adv.* **2023,** *9*, eadf4309.
(32) Keutsch, F. N.; Saykally, R. J. Water Clusters: Untangling the Mysteries of the Liquid, One Molecule at a Time. *Proc. Natl. Acad. Sci. U.S.A.* **2001,** *98*, 10533-10540.
(33) Zhang, B.; Yu, Y.; Zhang, Y.-Y.; Jiang, S.; Li, Q.; Hu, H.-S.; Li, G.; Zhao, Z.; Wang, C.; Xie, H., et al. Infrared Spectroscopy of Neutral Water Clusters at Finite Temperature: Evidence for a Noncyclic Pentamer. *Proc. Natl. Acad. Sci. U.S.A.* **2020,** *117*, 15423-15428.
(34) Xantheas, S. S.; Burnham, C. J.; Harrison, R. J. Development of Transferable Interaction Models for Water. II. Accurate Energetics of the First Few Water Clusters from First Principles. *J. Chem. Phys.* **2002,** *116*, 1493-1499.
(35) Pérez, C.; Muckle, M. T.; Zaleski, D. P.; Seifert, N. A.; Temelso, B.; Shields, G. C.; Kisiel, Z.; Pate, B. H. Structures of Cage, Prism, and Book Isomers of Water Hexamer from Broadband Rotational Spectroscopy. *Science* **2012,** *336*, 897-901.

(36) Temelso, B.; Archer, K. A.; Shields, G. C. Benchmark Structures and Binding Energies of Small Water Clusters with Anharmonicity Corrections. *J. Phys. Chem. A* **2011,** *115*, 12034-12046.
(37) Yuan, Q.; Cao, W.; Wang, X.-B. Cryogenic and Temperature-Dependent Photoelectron Spectroscopy of Metal Complexes. *Int. Rev. Phys. Chem.* **2020,** *39*, 83-108.
(38) Hanstorp, D.; Gustafsson, M. Determination of the Electron Affinity of Iodine. *J. Phys. B: At., Mol. Opt. Phys.* **1992,** *25*, 1773.
(39) Wang, X.-B.; Wang, L.-S. Photodetachment of Free Hexahalogenometallate Doubly Charged Anions in the Gas Phase: $[ML_6]^{2-}$, (M=Re, Os, Ir, Pt; L=Cl and Br). *J. Chem. Phys.* **1999,** *111*, 4497-4509.
(40) Lu, T. *Molclus Program*, 1.9.9.9; Beijing Kein Research Center for Natural Science: Beijing, China, 2018.
(41) Grimme, S.; Bannwarth, C.; Shushkov, P., A Robust and Accurate Tight-Binding Quantum Chemical Method for Structures, Vibrational Frequencies, and Noncovalent Interactions of Large Molecular Systems Parametrized for All Spd-Block Elements (*Z* = 1-86). *J. Chem. Theory Comput.* **2017**, *13*, 1989-2009.
(42) Pracht, P.; Bohle, F.; Grimme, S., Automated Exploration of the Low-Energy Chemical Space with Fast Quantum Chemical Methods. *Phys. Chem. Chem. Phys.* **2020**, *22*, 7169-7192.
(43) Grimme, S.; Hansen, A.; Ehlert, S.; Mewes, J.-M., r^2SCAN-3c: A "Swiss Army Knife" Composite Electronic-Structure Method. *J. Chem. Phys.* **2021**, *154*, 064103.
(44) Mehta, N.; Casanova-Páez, M.; Goerigk, L., Semi-Empirical or Non-Empirical Double-Hybrid Density Functionals: Which Are More Robust? *Phys. Chem. Chem. Phys.* **2018**, *20*, 23175-23194.
(45) Zheng, J.; Xu, X.; Truhlar, D. G., Minimally Augmented Karlsruhe Basis Sets. *Theor. Chem. Acc.* **2011**, *128*, 295-305.
(46) Adamo, C.; Barone, V., Toward Reliable Density Functional Methods without Adjustable Parameters: The PBE0 Model. *J. Chem. Phys.* **1999**, *110*, 6158-6170.
(47) Grimme, S.; Ehrlich, S.; Goerigk, L., Effect of the Damping Function in Dispersion Corrected Density Functional Theory. *J. Comput. Chem.* **2011**, *32*, 1456-1465.
(48) Woon, D. E.; Dunning, T. H., Gaussian Basis Sets for Use in Correlated Molecular Calculations. III. The Atoms Aluminum through Argon. *J. Chem. Phys.* **1993**, *98*, 1358-1371.
(49) Frisch, M. J.; Trucks, G. W.; Schlegel, H. B.; Scuseria, G. E.; Robb, M. A.; Cheeseman, J. R.; Scalmani, G.; Barone, V.; Petersson, G. A.; Nakatsuji, H., et al. *Gaussian 16 Rev. B.01*, Wallingford, CT, 2016.
(50) Riplinger, C.; Pinski, P.; Becker, U.; Valeev, E. F.; Neese, F., Sparse Maps-a Systematic Infrastructure for Reduced-Scaling Electronic Structure Methods. II. Linear Scaling Domain Based Pair Natural Orbital Coupled Cluster Theory. *J. Chem. Phys.* **2016**, *144*, 024109.
(51) Neese, F., The Orca Program System. *WIREs Comput. Mol. Sci.* **2012**, *2*, 73-78.
(52) Bayly, C. I.; Cieplak, P.; Cornell, W.; Kollman, P. A., A Well-Behaved Electrostatic Potential Based Method Using Charge Restraints for Deriving Atomic Charges: The RESP Model. *J. Phys. Chem.* **1993**, *97*, 10269-10280.
(53) Lu, T.; Chen, F., Multiwfn: A Multifunctional Wavefunction Analyzer. *J. Comput. Chem.* **2012**, *33*, 580-592.
(54) Hohenstein, E. G.; Sherrill, C. D., Density Fitting of Intramonomer Correlation Effects in Symmetry-Adapted Perturbation Theory. *J. Chem. Phys.* **2010**, *133*, 014101.

(55) Parker, T. M.; Burns, L. A.; Parrish, R. M.; Ryno, A. G.; Sherrill, C. D., Levels of Symmetry Adapted Perturbation Theory (SAPT). I. Efficiency and Performance for Interaction Energies. *J. Chem. Phys.* **2014**, *140*, 094106.
(56) Parrish, R. M., et al.; Burns, L. A.; Smith, D. G. A.; Simmonett, A. C.; DePrince, A. E., III; Hohenstein, E. G.; Bozkaya, U.; Sokolov, A. Y.; Di Remigio, R.; Richard, R. M., PSI4 1.1: An Open-Source Electronic Structure Program Emphasizing Automation, Advanced Libraries, and Interoperability. *J. Chem. Theory Comput.* **2017**, *13*, 3185-3197.
(57) Yuan, Q.; Rohdenburg, M.; Cao, W.; Aprà, E.; Landmann, J.; Finze, M.; Warneke, J.; Wang, X.-B. Isolated $[B_2(CN)_6]^{2-}$: Small Yet Exceptionally Stable Nonmetal Dianion. *J. Phys. Chem. Lett.* **2021**, *12*, 12005-12011.
(58) Jiang, Y.; Hu, Z.; Yang, Y.; Peng, P.; Zhong, C.; Sun, H.; Sun, Z.; Wang, X.-B. Beyond Duality: Rationalizing Repulsive Coulomb Barriers in Host–Guest Cyclodextrin–Dodecaborate Complexes. *J. Phys. Chem. Lett.* **2023**, *14*, 6736-6742.